Random-phase-approximation approach to collective modes around inhomogeneous Hartree-Fock states: One-dimensional doped Hubbard model

K. Yonemitsu, I. Batistić, and A. R. Bishop
Theoretical Division, Los Alamos National Laboratory, Los Alamos, New Mexico 87545
(Received 8 March 1991)

All the linear excitations are calculated in the random-phase approximation around a doped inhomogeneous Hartree-Fock state as well as the undoped uniform antiferromagnetic state in the one-dimensional Hubbard model. Upon doping, shape modes appear, localized around an introduced hole, as well as some "shake-off" branches related to combinations of local and extended Hartree-Fock orbitals. These modes are in addition to spin wave and ultragap branches in the pure antiferromagnetic state. Some characteristics of the shape modes are similar to bare processes in the t-t'-J model derived from the Hubbard model at strong coupling. Spectral weights in different susceptibility channels are calculated and shown to have peaks in low-energy regions, arising from specific shape modes.

I. INTRODUCTION

The description of quasiparticle excitations introduced by doping holes or electrons into broken-symmetry many-body ground states poses a central challenge for understanding the thermodynamics and response functions of many materials with strong correlations. Examples include self-trapped polaron (bag) states in charge-density-wave (CDW), spin-density-wave (SDW), or superconducting backgrounds, arising in models with strong electron-electron and/or electron-phonon interactions—models such as the Peierls or Hubbard Hamiltonians and their various extensions. These ideas are currently applied to a variety of electronic materials, particularly in reduced dimension, such as high-temperature superconductors and synthetic metals.

A number of many-body techniques are being applied to this issue, including analytic (e.g., variational, $1/N$ expansion, slave boson) and numerical (exact diagonalization, quantum Monte Carlo) approaches. The philosophy that we take here is that a reasonably accurate scheme maintaining flexibility and physical insight can play an important role in guiding the search for *appropriate* Hamiltonians in relation to specific materials. Thus, for instance, it is now clear that the doped half-filled 2D Hubbard model (much studied in the context of high-temperature cuprate superconductors[1]) is a highly "frustrated" system, which is an intrinsic problem for many techniques. The important question is how additional (physically motivated) terms added to the Hubbard model qualitatively change the doping states and their interaction—terms coming from a two-band description, electron-phonon interactions, for instance.

Here, we suggest that this qualitative level of understanding can be obtained by using random-phase-approximation (RPA), approach to adding linear fluctuations *around true Hartree-Fock (HF) solutions.* This gives access to quantization, and to both electronic and phonon response functions. RPA has been extensively studied in the context of *spatially uniform* ground states (e.g., a uniform CDW or SDW (Refs. [2–5])) where the fluctuations spectrum is composed of purely extended modes. Our main point here, however, is that RPA can be quite successful even in doped situations *if* the *true* HF state, which is in general spatially *inhomogeneous,* is used. Otherwise the RPA fluctuations must change the false HF state appropriately, except in weak coupling where the homogeneous HF state is approximately true. The same effect can be realized as a "dynamic renormalization" of the background[6]. The lesson is a familiar one in a field-theory context such as the quantization of solitons[7] (or the equivalent formulation of Bethe-Ansatz solvable models[8]), and leads to an RPA spectrum containing both spatially extended scattering states *and* localized modes. The localized modes carry the predominant "quasiparticle" information. In this sense the RPA is not a weak-coupling theory; *indeed* often improves with coupling strength and is useful even if strongly local structures in real space are present. Actually, a similar philosophy is now appearing in attempts to extend local-density-approximation (LDA) band structure to incorporate many-body corrections—perturbative corrections are added to the (HF level) LDA band structure with good success in some test cases.[9]

We have begun to apply this approach to several model Hamiltonians in 1D and 2D, including one-band and two-band extended Peierls-Hubbard models. In this paper we focus on the method and its application to a "simple" example, the 1D pure Hubbard model. This is a convenient test case because it has been studied extensively by many other techniques, and some properties are known exactly via the Bethe-Ansatz[10] or equivalent methods. This model shows that doped inhomogeneous HF solutions produce spatially localized modes as well as extended ones, in the linear excitation spectra. The localized modes play important roles in determining quasiparticle properties in appropriate susceptibility channels.

The present method, which has been developed by Bohm and Pines[11] in the description of plasma oscillations and by Thouless[12] in a nuclear physics context, consists in diagonalization for all particle-hole pair excitations, regarding them as bosons. When Ne electrons exist

in the N-site system, there are $(2N-Ne)$ particle states, Ne hole states, and therefore $(2N-Ne)Ne$ particle-hole pairs. Considering creation and annihilation of all the pairs, we have to diagonalize a $2(2N-Ne)Ne \times 2(2N-Ne)Ne$ matrix. The size of the matrix may be reduced if the HF solution has some symmetry, which is not assumed here for arbitrary inhomogeneous HF solutions.

As noted above, the present formulation has been more familiar in nuclear physics. Its main advantage is that eigenmodes obtained here do not depend on frequency because *all* linear excitations are calculated. Thus it is easy to obtain correlation functions within the RPA at *any* frequency after solution of the eigenvalue problem for particle-hole pair excitations. This is in contrast to the other methods[13,14], where "bare correlation functions" or bubble diagrams are summed infinitely by using a $2N \times 2N$ matrix for the one-band Hubbard model. Components of the matrix describe sites and spins. In these methods, eigenmodes depend on frequency, and therefore correlation functions are calculated at each frequency. Such methods are powerful for the pure one-hand Hubbard model because exchange interactions need not be considered. More generally, the importance of exchange interactions depends on the specific model. However, in our approach they are automatically included on the same footing as the direct interaction contributions.

When extended Hubbard interactions are studied, for example coupling with phonons or longer-range interactions, the present method is useful in the sense that these interactions are taken into account on the same footing. For example, exchange interactions are treated in the same way as direct interactions. When electron-phonon interactions are considered, particle-hole pair excitations and phonons are treated equally. Some phonons may be coupled with magnons, for example. The present method is especially useful when detailed information on eigenfunctions and eigenfunctions are necessary, for example, in the study of Raman spectra. It also makes sure that information is not lost by selective frequency searches.

The major disadvantage of the present method is that the matrix to be diagonalized has much larger dimensions.

The outline of this paper is as follows: the formulation is presented in Sec. II, and compared with the linear spin-wave theory for the spin-$\frac{1}{2}$ antiferromagnetic (AF) Heisenberg model in Sec. III. In Sec. IV, results are presented for the one-hole case as well as the half-filled case and compared with the t-t'-J model. Section V contains a summary and some remaining issues.

II. HARTREE-FOCK AND RANDOM PHASE APPROXIMATIONS

In this paper, we study the one-dimensional, one-band Hubbard model,

$$H=-t\sum_{i,\alpha}(c_{i\alpha}^{\dagger}c_{i+1\alpha}+c_{i+1\alpha}^{\dagger}c_{i\alpha})+U\sum_{i}c_{i\uparrow}^{\dagger}c_{i\uparrow}c_{i\downarrow}^{\dagger}c_{i\downarrow}\ , \tag{1}$$

with periodic boundary condition $c_{N+1\alpha}=c_{1\alpha}$, where N is the number of sites. As a first step we solve the unrestricted Hartree-Fock (HF) Hamiltonian,

$$H_{\rm HF}=-t\sum_{i,\alpha}(c_{i\alpha}^{\dagger}c_{i+1\alpha}+c_{i+1\alpha}^{\dagger}c_{i\alpha})+\frac{U}{2}\sum_{i}(q_i\hat{\rho}_i-\mathbf{m}_i\hat{\sigma}_i)-\frac{U}{4}\sum_{i}(q_i^2-\mathbf{m}_i^2)\ , \tag{2}$$

with the self-consistency conditions

$$q_i=\langle\hat{\rho}_i\rangle_{\rm HF},\quad \mathbf{m}_i=\langle\hat{\sigma}_i\rangle_{\rm HF}\ , \tag{3}$$

where $\hat{\rho}_i=\sum_{\alpha}c_{i\alpha}^{\dagger}c_{i\alpha}$, $\hat{\sigma}_i=\sum_{\alpha,\beta}c_{i\alpha}^{\dagger}\boldsymbol{\sigma}_{\alpha\beta}c_{i\beta}$, $\boldsymbol{\sigma}$ stands for Pauli matrices, and $\langle\ \rangle_{\rm HF}$ denotes the expectation value in the HF state.

Next we go beyond the HF approximation. Creation of particles and holes are defined by creation of unoccupied HF orbitals and annihilation of occupied ones, respectively. Then $H-H_{\rm HF}$ contains various terms, representing scatterings of particle-particle (p-p), hole-hole (h-h), or particle hole (p-h) pairs, creation or annihilation of p-h pairs, and scattering of a particle or hole accompanied by creation or annihilation of a p-h pair. When only those terms are retained which represent scattering, creation or annihilation of p-h pairs, the boson Hamiltonian $H_{\rm RPA}$ is obtained.[15]. Then we diagonalize the boson Hamiltonian,

$$H_{\rm RPA}=\sum_{\lambda>F>\mu}(\varepsilon_{\lambda}-\varepsilon_{\mu})\xi_{\lambda\mu}^{\dagger}\xi_{\lambda\mu}+\sum_{\lambda\nu>F>\mu\tau}(v_{\lambda\mu\nu\tau}^{*}\xi_{\lambda\mu}^{\dagger}\xi_{\nu\tau}+\tfrac{1}{2}u_{\lambda\mu\nu\tau}^{*}\xi_{\lambda\mu}^{\dagger}\xi_{\nu\tau}^{\dagger}+\tfrac{1}{2}u_{\lambda\mu\nu\tau}\xi_{\lambda\mu}\xi_{\nu\tau})\ , \tag{4}$$

where

$$v_{\lambda\mu\nu\tau}^{*}=U\sum_{i}(\phi_{\lambda}^{*}(i\uparrow)\phi_{\tau}^{*}(i\downarrow)-\phi_{\lambda}^{*}(i\downarrow)\phi_{\tau}^{*}(i\uparrow)\times(\phi_{\mu}(i\uparrow)\phi_{\nu}(i\downarrow)-\phi_{\mu}(i\downarrow)\phi_{\nu}(i\uparrow))\ , \tag{5}$$

$$u_{\lambda\mu\nu\tau}^{*}=U\sum_{i}(\phi_{\lambda}^{*}(i\uparrow)\phi_{\nu}^{*}(i\downarrow)-\phi_{\lambda}^{*}(i\downarrow)\phi_{\nu}^{*}(i\uparrow))\times(\phi_{\mu}(i\uparrow)\phi_{\tau}(i\downarrow)-\phi_{\mu}(i\downarrow)\phi_{\tau}(i\uparrow))\ , \tag{6}$$

and ε_{λ} and $\phi_{\lambda}(i\alpha)$ are the energy level and orbital obtained from the HF Hamiltonian $H_{\rm HF}$. The operator $\xi_{\lambda\mu}^{\dagger}$ stands for creation of an unoccupied HF orbital λ and annihilation of an occupied HF orbital μ, $\xi_{\lambda\mu}^{\dagger}=c_{\lambda}^{\dagger}c_{\mu}$, and is regarded as a boson creation operator.

$$[\xi_{\lambda\mu},\xi_{\nu\tau}^{\dagger}]\simeq\langle[\xi_{\lambda\mu},\xi_{\nu\tau}^{\dagger}]\rangle_{\rm HF}=\delta_{\lambda\nu}\delta_{\mu\tau}\ , \tag{7}$$

$$[\xi_{\lambda\mu},\xi_{\nu\tau}]\simeq\langle[\xi_{\lambda\mu},\xi_{\nu\tau}]\rangle_{\rm HF}=0\ . \tag{8}$$

Here the indices λ and ν denote unoccupied HF orbitals, and μ and τ denote occupied ones. Commutation relations of $\xi_{\lambda\mu}^{\dagger}$ and $\xi_{\nu\tau}$ are approximated by taking their expectation values in the HF state, thus the operators are regarded as pure boson operators. The first term of the boson Hamiltonian $H_{\rm HPA}$ is derived so as to give the same commutation relations with $\xi_{\lambda\mu}^{\dagger}$ and $\xi_{\nu\tau}$ as the HF Hamiltonian $H_{\rm HF}$, when Eqs. (7) and (8) are used for the

former. Equations of motion of p-h pair excitations around the HF state have thus been linearized by retaining the linear terms with respect to $\zeta^\dagger_{\lambda\mu}$ and $\zeta_{\nu\tau}$:

$$\omega_n \xi^\dagger_n = [H_{\mathrm{RPA}}, \xi^\dagger_n] , \tag{9}$$

where

$$\xi^\dagger_n = \sum_{\lambda > F > \mu} (\psi^{(n)*}_{\lambda\mu} \zeta^\dagger_{\lambda\mu} - \varphi^{(n)*}_{\lambda\mu} \zeta_{\lambda\mu}) , \tag{10}$$

with n labeling an eigenmode in the linear excitation spectra.

The two-body Green function is generally written, by the Lehmann representation, as

$$\Pi_{\lambda\mu\nu\tau}(\omega) \equiv -i \int_{-\infty}^{\infty} dt\, e^{i\omega t} \langle 0 | \mathcal{T} c^\dagger_\mu(t) c_\lambda(t) c^\dagger_\nu c_\tau | 0 \rangle$$
$$= \sum_n \left[\frac{\langle 0|c^\dagger_\mu c_\lambda|n\rangle \langle n|c^\dagger_\nu c_\tau|0\rangle}{\omega - (E_n - E_0) + i\eta} - \frac{\langle 0|c^\dagger_\nu c_\tau|n\rangle \langle n|c^\dagger_\mu c_\lambda|0\rangle}{\omega + (E_n - E_0) - i\eta} \right] . \tag{11}$$

Here, the indices are *not* restricted to either unoccupied or occupied HF orbitals. The symbol η denotes an infinitesimally small positive number. We obtain this quantity within the RPA by solving Eqs. (9) and (10) and identifying $|n\rangle$ and $(E_n - E_0)$ with $\xi^\dagger_n|0\rangle$ and ω_n, respectively. Here $|0\rangle$ is the RPA ground state defined by $\xi_n|0\rangle = 0$. The matrix element $\langle 0|c^\dagger_\mu c_\lambda|n\rangle$ is given by

$$\langle 0|c^\dagger_\mu c_\lambda|n\rangle = \begin{cases} \psi^{(n)*}_{\lambda\mu} & \text{if } \lambda > F > \mu , \\ \varphi^{(n)*}_{\mu\lambda} & \text{if } \mu > F > \lambda , \\ 0 & \text{otherwise} . \end{cases} \tag{12}$$

Equivalence between this method and the usual diagrammatic RPA method has been derived in Ref. [12]. It has also been shown there that the RPA Green function thus obtained satisfies the sum rule, which relates the frequency integration of the retarded RPA Green function, weighted by ω, to the expectation value of the double commutator in the state $|0\rangle$. Of course, the exact integrated spectral weight may differ from the RPA estimate, particularly because of additional processes at $\omega \gtrsim$ the HF excitation gap ($\sim U \gg t$)—this will need to be assessed for each specific model Hamiltonian.

III. COMPARISON WITH LINEAR SPIN-WAVE THEORY

The large-U half-filled Hubbard model is reduced, to $O(t^2/U)$, to the spin-$\frac{1}{2}$ antiferromagnetic (AF) Heisenberg model with exchange coupling $J = 4t^2/U$. In the infinite U limit, the HF solution is the spin-density-wave state with saturated staggered magnetization or the classical Néel state. HF orbitals can be chosen to be localized at a given site because of degeneracy in this case. Then the operator $\zeta^\dagger_{\lambda\mu} = c^\dagger_\lambda c_\mu$ is reduced to $c^\dagger_{2m\downarrow} c_{2n\uparrow}$, $c^\dagger_{2m+1\uparrow} c_{2n+1\downarrow}$, $c^\dagger_{2m\downarrow} c_{2n+1\downarrow}$, or $c^\dagger_{2m+1\uparrow} c_{2n\uparrow}$ when $m^z_i = (-1)^i$. On the other hand, in the linear spin-wave theory[16] of the Heisenberg model, the spin operators are described with the use of boson operators $a_i a^\dagger_i, b_i, b^\dagger_i$ as $S^-_{2n} \equiv c^\dagger_{2n\downarrow} c_{2n\uparrow} = a^\dagger_{2n}$ and $S^+_{2n+1} \equiv c^\dagger_{2n+1\uparrow} c_{2n+1\downarrow} = b^\dagger_{2n+1}$ in the antiferromagnetic case with spin $\frac{1}{2}$. In one dimension, the RPA excitation spectrum has been obtained for the half-filled Hubbard model[2,3], and the dispersion relation and the eigenfunctions for the excitations with low-energy $O(t^2/U)$ have been shown, in the large-U limit, to be the same as those in the linear spin-wave theory of the 1D spin-$\frac{1}{2}$ AF Heisenberg model.

It has been found, in the 2D half-filled Hubbard model, that the spin-wave spectrum, staggered magnetization and ground-state energy obtained in the large-U limit in the RPA are the same as those obtained in the linear spin-wave theory[5,13,17]. In analysis of self-energy correction within the RPA, (Refs. [17] and [18]), the lowest-energy state for a hole added to the 2D half-filled Hubbard model has been shown to be the $k = (\pm\pi/2, \pm\pi/2)$ state, as found in the t-t'-J model.[19]. Interaction of holes via transverse spin fluctuations within the RPA has been reduced[20], to $O(t^2/U)$, to that given for the t-J model.[21] These RPA results have been obtained for linear excitations around the uniform AF state. Some linear excitations around inhomogeneous HF solutions have been investigated recently.[13,14]

The linear spin-wave theory for the AF Heisenberg model not only works well in 2D ($T = 0$) and 3D, but also gives good estimation of the total ground-state energy even in 1D, even though the 1D model does not have long-range order. Thus the RPA may give fairly good results for some quantities for large U, though it is essentially a weak-coupling theory taking only linear fluctuations around HF solutions.

The linear spin-wave theory is known to give a logarithmic divergence for reduction of the staggered magnetization and equal-time correlation function of transverse spins, in 1D at $T = 0$ and in 2D at $T > 0$, reflecting the absence of long-range order. We have calculated the equal-time correlation function of transverse spins in the 1D finite-U half-filled Hubbard model, in the RPA with the exclusion of zero-frequency modes. This also shows a logarithmic divergence with respect to the system size N. The divergence in the reduction of the long-range order means that the RPA fluctuations overcompensate the broken symmetry.

There is another less serious problem related to zero-frequency modes, which always exist when the continuous symmetry possessed by the Hamiltonian is broken in the HF solution, as shown later in Sec. IV. These modes attempt to restore the broken symmetry. They give divergent results for the two-body Green functions if the matrix elements between them and the RPA ground state

are finite, although they may be neglected in the thermodynamic limit. The linearization treatment given in the RPA is not sufficient for the zero-frequency modes. It would be necessary for these to be treated differently than finite frequency modes, as in quantization about classical nonlinear fields.[7] In the present study, we introduce a very small positive number (10^{-10}) into the matrix elements which are related to the zero-frequency modes in order to avoid numerical instability. Thus the zero-frequency modes have very small but finite frequencies ($\omega_n < 10^{-5}$) and are treated in the same way as the other modes.

IV. RESULTS

Here we present explicit results for the 1D Hubbard model. The energy is given in units of t. We have first obtained HF solutions with different U values. When a hole is introduced into the half-filled system, a kink appears for small U ($\leq 5t$) and a kink-antikink bound state for large U ($\geq 8t$). Here a kink-antikink bound state should be distinguished from the spin bag (polaron).[5] This is because spin density has an opposite sign at the site where a hole is localized so that a kink and an antikink are considered to be tightly bound around the hole. There is an additional twist with a uniform pitch if necessitated by the boundary condition. Solutions in the intermediate U regime ($5.5t \leq U \leq 7.5t$) interpolate smoothly between these two kinds of solutions, that is, have phase jumps intermediate between π and 2π at the defect, where the phase is defined with respect to the staggered magnetization. For very large U ($\geq 12t$ when $N=12$, $\geq 9t$ when $N=11$), a ferromagnetic core appears around the hole. This is reminiscent of a Nagaoka ferromagnetic state in the infinite-U limit with one hole,[22] and indeed the "ferromagnetic" core increases in size with increasing U. However, the state obtained here is not completely ferromagnetic. The critical interaction strength for the appearance of the ferromagnetic core depends strongly on the system size.

We also calculate the correction to the HF ground-state energy. It is given by the c-number term produced in the course of diagonalization of the boson Hamiltonian H_{RPA}.[3,23] When the interaction U is absent, the correction is zero because the HF ground-state energy is of course correct. In the half-filled case, the RPA overestimates the correction by about twice as much as the exact one for small U ($\lesssim 3t$). When U is about $4t$, where the energy difference between the HF result and the exact one is the largest, the RPA overestimates the correction by a factor of about 1.5. As the interaction strength U becomes larger, the RPA gives increasingly better results. The interaction strength $U/t=8$, for which we choose to show results here, is a region where the correction to the HF ground-state energy is overestimated in the RPA by a factor of about 1.1. When the interaction strength U is extremely large ($U \geq 20t$), the comparison between the results for the half-filled cases with $N=6$, 8 obtained in the RPA and by exact diagonalization shows that the RPA slightly underestimates the correction by a few percent, as found in the linear spin-wave theory for the 1D spin-$\frac{1}{2}$ AF Heisenberg model in the thermodynamic limit.[16] Comparison of our results for the *one*-hole system (with $N=16$ and $U/t=8$) with Bethe-Ansatz thermodynamic results, at the corresponding density, shows that our RPA underestimates the correction to the HF ground-state energy by approximately 15%.

All the energies of the linear excitations are plotted in increasing order in Fig. 1, for the half-filled system (a), and for the one-hole system (b), with interaction strength $U/t=8$ and system size $N=16$. When only the z component of the spin densities m_i^{μ}, $\mu=x,y,z$, is nonzero, as in the cases shown in Fig. 1, the nth excited $|n\rangle$ is called a transverse spin mode if $\langle 0|\hat{\sigma}_i^x|n\rangle$ or $\langle 0|\hat{\sigma}_i^y|n\rangle$ is finite for some i, a longitudinal spin mode if $\langle 0|\hat{\sigma}_i^z|n\rangle$ is finite, or a charge mode if $\langle 0|\hat{\rho}_i|n\rangle$ is finite. In case (b), a longitudinal spin (charge) mode is mixed with charge (longitudinal spin) modes to varying degrees.

A. Character of linear excitations in the half-filled case

In the half-filled case [Fig. 1(a)], low-lying linear excitations are transverse spin modes and called spin-wave modes.[2,3] The lowest two linear excitations are Goldstone modes, which have zero energy and are related to restoration of the spin rotation symmetry which is broken in the HF solution. Higher-energy linear excitations

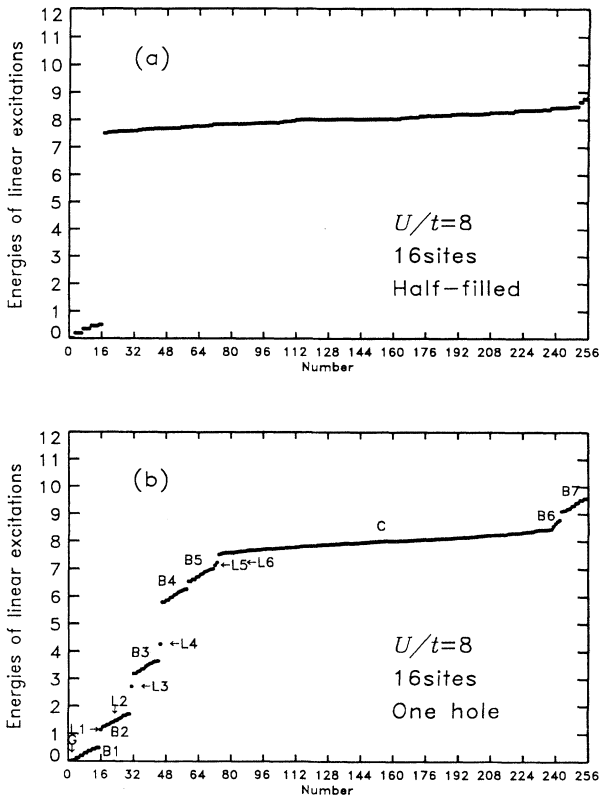

FIG. 1. Energies of the linear excitations for $U/t=8$ and $N=16$. (a) Half-filled system. (b) One-hole system. The symbols B,C,G,L denote branch, continuum, Goldstone mode, and localized mode, respectively.

are either charge, longitudinal spin or transverse spin modes. The lowest energy of the latter is 7.51, which is the same within numerical accuracy as the energy difference 2Δ between the lowest unoccupied HF orbital and the highest occupied one. The highest five linear excitations have energies ($8.64 \leq \omega_n \leq 8.80$) larger than the energy difference between the highest and lowest HF orbitals (8.51). These "ultragap" modes all have pure charge character. We call the modes which are different from the spin-wave or the ultragap modes the modes in the continuum.

In order to see what process is important in each linear excitation, we have calculated

$$w^n(\hat{O},l)=\frac{1}{N}\sum_{i=1}^{N}|\langle 0|\hat{O}_{i+l,i}|n\rangle|^2 , \tag{13}$$

where $\hat{O}_{i+l,i}$ is one of the following

$$\hat{\rho}_{i+l,i}=\tfrac{1}{2}\sum_{\alpha} c^{\dagger}_{i+l\alpha}c_{i\alpha}+\text{H.c.} , \tag{14}$$

$$\hat{\sigma}^{\gamma}_{i+l,i}=\tfrac{1}{2}\sum_{\alpha,\beta} c^{\dagger}_{i+l\alpha}\sigma^{\gamma}_{\alpha\beta}c_{i\beta}+\text{H.c.} \quad (\gamma=x,y,z) , \tag{15}$$

$$\hat{j}_{i+l,i}=\frac{-i}{2}\sum_{\alpha} c^{\dagger}_{i+l\alpha}c_{i\alpha}+\text{H.c.} , \tag{16}$$

$$\hat{j}^{\gamma}_{i+l,i}=\frac{-i}{2}\sum_{\alpha,\beta} c^{\dagger}_{i+l\alpha}\sigma^{\gamma}_{\alpha\beta}c_{i\beta}+\text{H.c.} \quad (\gamma=x,y,z) . \tag{17}$$

The operators $\hat{\rho}_{i,i}$ and $\hat{\sigma}^{\gamma}_{i,i}$ are the previously defined charge- and spin-density operators $\hat{\rho}_{i,i}=\hat{\rho}_i, \hat{\sigma}^{\gamma}_{i,i}=\hat{\sigma}^{\gamma}_i$, respectively. The operators $\hat{\rho}_{i+l,i}$ and $\hat{\sigma}^{\gamma}_{i+l,i}$ ($l\neq 0$) are regarded as generalized charge- and spin-density operators, respectively. For example, $\hat{\rho}_{i+1,i}$ is a bond-charge-density operator. The operators $\hat{j}_{i+1,i}$ and $\hat{j}^{\gamma}_{i+1,i}$ are proportional to charge and spin current operators, respectively, while $\hat{j}_{i+l,i}$ and $\hat{j}^{\gamma}_{i+l,i}$ ($l\neq 1$) are regarded as generalized current operators.

The spin-wave modes have large amplitude only in $w^n(\hat{\sigma}^x,l=0)$ and $w^n(\hat{\sigma}^y,l=0)$. The dominant process in the spin-wave modes is, therefore, annihilation of up (down) spin at a given site and creation of down (up) spin at the same site, or spin flip without hopping which is consistent with the usual picture in the linear spin-wave theory for the Heisenberg antiferromagnet. The ultragap modes have their largest amplitude in the process of hopping to the nearest-neighbor sites without spin flip $w^n(\hat{j},l=1)$, or charge transfer to the nearest-neighbor sites. The transverse spin modes in the continuum have large amplitude in $w^n(\hat{O},l)$ for $\hat{O}=\hat{\sigma}^x,\hat{\sigma}^y,\hat{j}^x$, or $\hat{j}^y$ and $l=2n$ ($n\neq 0$), while the longitudinal spin and charge modes in the continuum for $\hat{O}=\hat{\sigma}^z,\hat{\rho},\hat{j}^z$, or $\hat{j}$ and $l=2n+1$. Unlike the spin-wave modes or the ultragap modes, the continuum mode processes are not limited to a particular process with respect to the hopping distance l. If spins are flipped, they hop to the same sublattice. If not, they hop to the other sublattice. They are consistent with the Pauli principle. The cost energy about $2\Delta \simeq U$ in the large-U regime.

In order to study total and relative momenta for each linear excitation, we calculated $w^{+n}(\hat{O},p)$ and $w^{-n}(\hat{O},p)$, respectively, where

$$w^{\pm n}(\hat{O},p)=\frac{1}{N}\sum_{k}|\langle 0|\hat{O}_{\pm k,k+p}|n\rangle|^2 , \tag{18}$$

and $\hat{O}_{k,k+p}$ is $\hat{\rho}_{k,k+p}=\sum_{\alpha} c^{\dagger}_{k\alpha}c_{k+p\alpha}$, or $\hat{\sigma}^{\gamma}_{k,k+p}=\sum_{\alpha,\beta} c^{\dagger}_{k\alpha}\sigma^{\gamma}_{\alpha\beta}c_{k+p\beta}$ ($\gamma=x,y,z$). Here the operators $c^{\dagger}_{k\alpha}$ and $c_{k\alpha}$ are Fourier transforms of $c^{\dagger}_{i\alpha}$ and $c_{i\alpha}$, respectively. The total momentum is a good quantum number if p and $p+\pi$ are not distinguished in the half-filled case. Because of degeneracy between p and $-p$, each mode has amplitude only in $w^{+n}(\hat{O},q)$ for $q=\pm p, \pm p+\pi$. Meanwhile, distribution of the relative momentum in $w^{-n}(\hat{O},q)$ is not restricted to particular q's, except for the fact that modes with total momenta $2\pi(2n)/N$ or $2\pi(2n+1)/N$ are only associated with relative momenta $2\pi(2m)/N$ or $2\pi(2m+1)/N$, respectively, due to the definition of these momenta.

For the spin-wave modes, p-h pairs with different relative momenta contribute with similar weights. In the large-U limit, they contribute with equal weights. Precisely speaking, in this limit the p-h pair (λ,μ)'s with a given total momentum (modulo π) and opposite spins (in terms of c and $c^{\dagger}$ operators) have a constant value for $\psi^{(n)*}_{\lambda\mu}$'s and another constant value for $\varphi^{(n)*}_{\lambda\mu}$'s, where different (λ,μ)'s correspond to different relative momenta.[3] The ultragap modes have contributions from p-h pairs with various relative momenta, too. Meanwhile, the modes in the continuum have contributions mainly from p-h pairs with relative momenta $\pm p$, $\pm p+\pi$ for a certain value of p. This means that interaction between p-h pairs with different momenta is weak for the modes in the continuum. The continuum may be described almost by the free p-h continuum.[3] Note the "step" structure in the continuum related to the finite number of sites.

B. Character of linear excitations in the one-hole case

In the one-hole case [Fig. 1(b)], the HF solution is a kink-antikink bound state with a localized hole at the 16th or 0th site as shown in Fig. 2. The HF energy levels are plotted in increasing order in Fig. 3. The lowest fifteen HF orbitals are occupied.

The RPA excitation spectrum [Fig. 1(b)] now contains both *local* and *extended* modes, which we discuss in detail below. A feature is the appearance of branches of more extended modes accompanying the localized gap modes—these are analogous to "shake-off" spectra in electron-phonon coupled systems,[24] but here built from spin and charge fluctuations.

The 1st and 16th HF orbitals are local orbitals with down spin and even parity with respect to the location of the hole. The 17th, 18th, and 19th HF orbitals are also local orbitals with up spin and even, odd, and even parities, respectively. These orbitals can be understood if the 15th(=−1st), 16th(=0th), and 1st sites are considered to have equal magnitude of charge density q and negative spin density $-m$ and if hopping of electrons between the 14th and 15th sites and the 1st and 2nd sites are neglected. With this approximation, HF energy levels and HF orbitals are obtained as shown in Table I. The 1st and

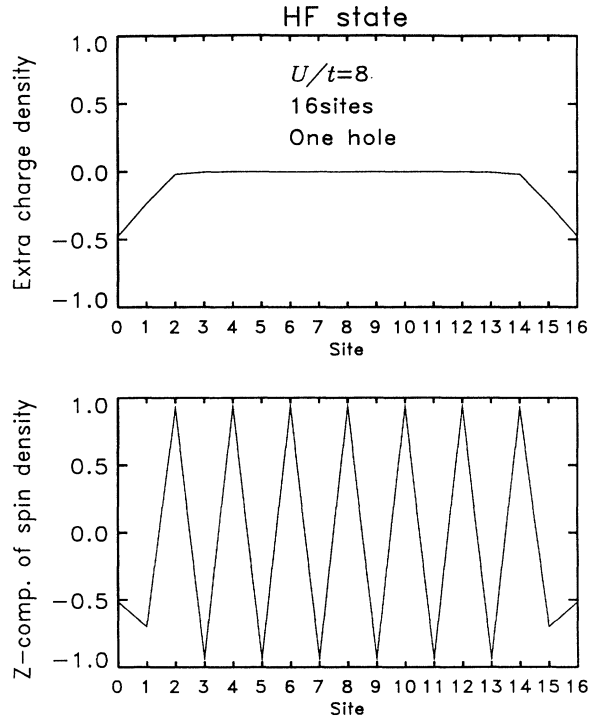

FIG. 2. The extra charge density, $q_i - 1$ (upper part) and the z component of the spin density, m_i^z (lower part), in the HF state of the one-hole system for $U/t = 8$ and $N = 16$.

16th to 19th local HF orbitals correspond to the 1st and 3rd to 6th orbitals, respectively, from bottom to top of Table I. However, the local HF orbital is missing which corresponds to the second one of Table I with down spin and odd parity. The 5th, 9th, 13th, and 15th HF orbitals have down spin and odd parity in the occupied ones, but

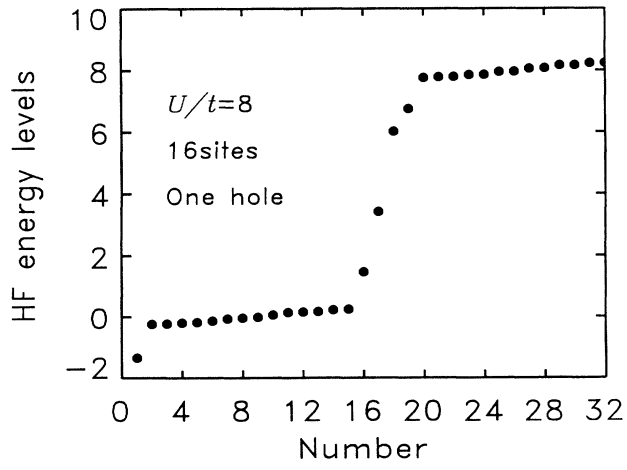

FIG. 3. The HF energy levels in the one-hole system for $U/t = 8$ and $N = 16$.

TABLE I. HF solution in the three-site approximation.

HF energy levels	HF orbitals		
$\frac{U}{2}(q+m)+\sqrt{2t}$	$\frac{1}{\sqrt{6}}(-\lvert-1\uparrow\rangle$	$+\sqrt{2}\lvert 0\uparrow\rangle$	$-\lvert+1\uparrow\rangle)$
$\frac{U}{2}(q+m)$	$\frac{1}{\sqrt{2}}(+\lvert-1\uparrow\rangle$		$-\lvert+1\uparrow\rangle)$
$\frac{U}{2}(q+m)-\sqrt{2t}$	$\frac{1}{\sqrt{6}}(+\lvert-1\uparrow\rangle$	$+\sqrt{2}\lvert 0\uparrow\rangle$	$+\lvert+1\uparrow\rangle)$
$\frac{U}{2}(q-m)+\sqrt{2t}$	$\frac{1}{\sqrt{6}}(-\lvert-1\downarrow\rangle)$	$+\sqrt{2}\lvert 0\downarrow\rangle$	$-\lvert+1\downarrow\rangle)$
$\frac{U}{2}(q-m)$	$\frac{1}{\sqrt{2}}(+\lvert-1\downarrow\rangle$		$-\lvert+1\downarrow\rangle)$
$\frac{U}{2}(q-m)-\sqrt{2t}$	$\frac{1}{\sqrt{6}}(+\lvert-1\downarrow\rangle$	$+\sqrt{2}\lvert 0\downarrow\rangle$	$+\lvert+1\downarrow\rangle)$

they are extended through the whole system.

The lowest fifteen linear excitations ($B1$) are transverse spin modes (spin-wave modes), which are distorted in the vicinity of the hole. Only the first, G, is a Goldstone mode. This has zero energy and is related to restoration of the spin rotation symmetry which is broken in the HF solution. The i dependence of $\langle 0|\hat{O}_i|n\rangle$ for the Goldstone mode ($n=1$) is shown in Fig. 4(a), where $\hat{O}_i$ is $\hat{\sigma}_i^x$ (upper part) and $\hat{\sigma}_i^y$ (lower part). The quantities $\langle 0|\hat{O}_i|n\rangle$ with $\hat{O}_i$ being $\hat{\rho}_i$ or $\hat{\sigma}_i^z$ are zero. Real and imaginary parts are represented by solid and dashed lines, respectively. The mode has even parity with respect to the location of the hole. The spin-density profile is the same as in Fig. 2, but appears in the perpendicular direction to the HF spin density. The dominant process in the spin-wave modes, which include the Goldstone mode, is spin flip without hopping, as in the case of Fig. 1(a). The spin-wave modes have contributions from various p-h pairs.

The 16th linear excitation, $L1$, can be viewed as a *translational* shape mode, as shown in Fig. 4(b), a spatially *localized* mixed mode of charge and longitudinal spin with odd parity. This mode has energy 1.14, slightly less than the energy difference between the lowest unoccupied HF orbital and the highest occupied one at 1.23. Its dominant process is annihilation and creation of an electron without flip or hopping [$w^{16}(\hat{\rho}$ and $\hat{\sigma}^z, l=0)$]. Hopping to the nearest-neighbor sites without spin flip [$w^{16}(\hat{\rho},\hat{\sigma}^z,\hat{j}$ and $\hat{j}^z, l=1)$] is the next most dominant process. Hopping to the next-nearest-neighbor sites [$w^{16}(\hat{j}$ and $\hat{j}^z, l=2)$] is also comparable. The processes with $l=0,2$ are induced by the reduction of charge density around the hole. This mode has contributions mainly from the p-h pairs associated with the 16th local HF orbital for a particle state and with the 15th, 13th, 9th, and 5th extended HF orbitals for hole states. Some linear combination of these extended HF orbitals may be viewed as the missing local HF orbital when the local HF orbitals are analyzed within the three-site approximation (Table I).

The thirteen linear excitations, from the 17th mode to the 30th mode, excluding the 22nd mode, form a branch, $B2$. They have contributions mainly from the p-h pair associated with the 16th local HF orbital and one of the fourteen extended occupied HF orbitals. Each mode on

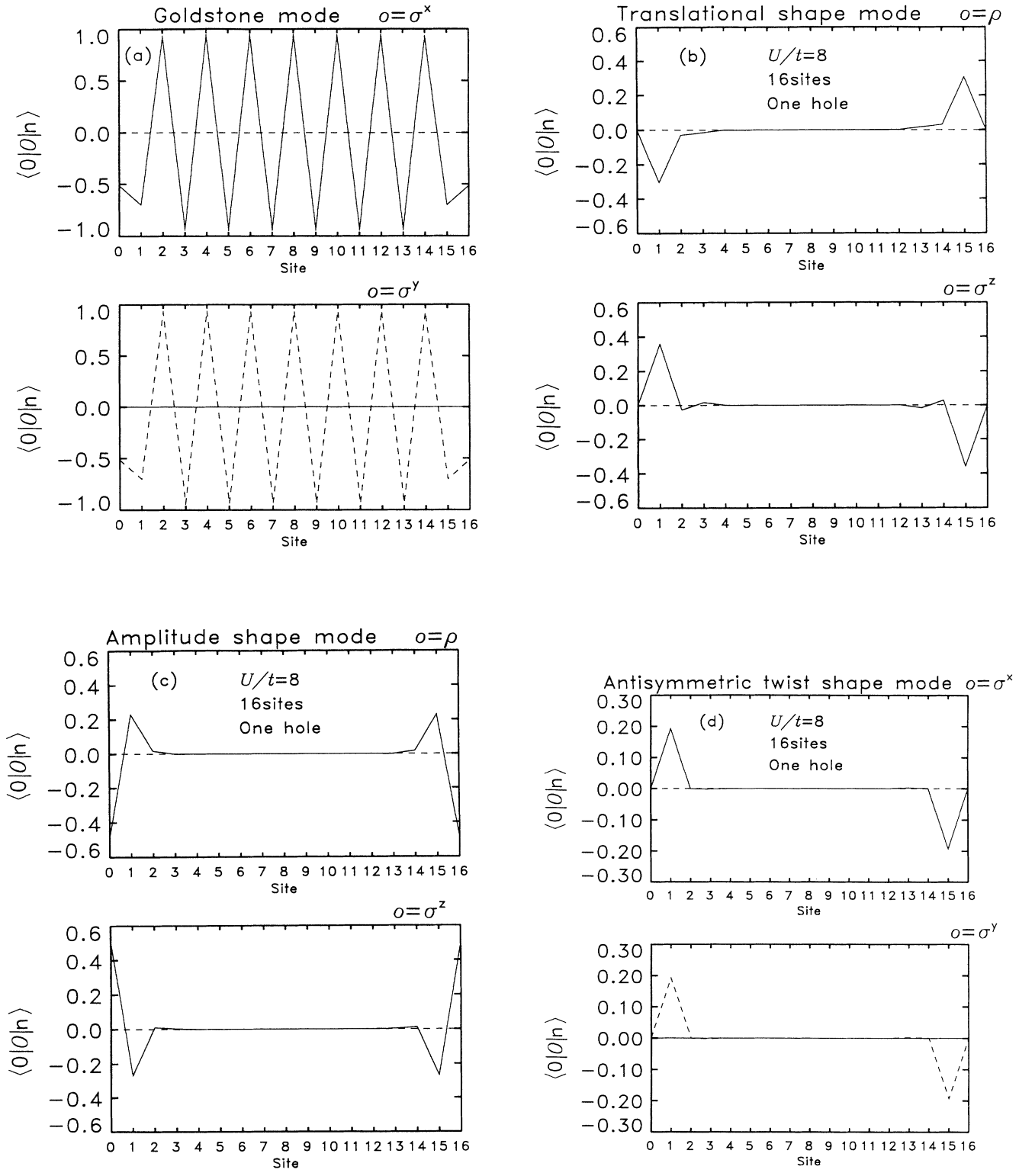

FIG. 4. The quantity $\langle 0|\hat{O}_i|n\rangle$ in the one-hole system for $U/t=8$ and $N=16$. Real and imaginary parts are represented by solid and dashed lines, respectively. (a) $\hat{O}_i=\hat{\sigma}_i^x$ (upper part) and $\hat{O}_i=\hat{\sigma}_i^y$ (lower part) for the Goldstone model ($n=1$). (b) $\hat{O}_i=\hat{\rho}_i$ (upper part) and $\hat{O}_i=\hat{\sigma}_i^z$ (lower part) for the translational shape mode ($n=16$). (c) $\hat{O}_i=\hat{\rho}_i$ (upper part) and $\hat{O}_i=\hat{\sigma}_i^z$ (lower part) for the amplitude shape mode ($n=31$). (d) $\hat{O}_i=\hat{\sigma}_i^x$ (upper part) and $\hat{O}_i=\hat{\sigma}_i^y$ (lower part) for the antisymmetric twist shape mode ($n=45$).

this branch has a main process of hopping to a certain site, which depends on the mode, with or without spin flip. There is no restriction on the hopping distance l, in contrast to the case of Fig. 1(a), where transverse spin modes have even numbers l and longitudinal spin and charge modes have odd numbers l.

The 22nd linear excitation, $L2$ is a symmetric *twist* shape mode, which is a spatially *localized* transverse spin mode with even parity. This mode has energy 1.41, within the region of the branch $B2$. Its main process is spin flip without hopping [$w^{22}(\hat{\sigma}^x$ and $\hat{\sigma}^y, l=0)$]. This mode has contributions mainly from the p-h pair associated with the 17th and 1st local HF orbitals. Thus, it is distinct from the modes in the branch $B2$.

The 31st linear excitation, $L3$, is an *amplitude* shape mode, as shown in Fig. 4(c), a spatially *localized* mixed mode of charge and longitudinal spin with even parity. This mode has energy 2.71. Its processes are similar to those in the translational shape mode. The main process is annihilation and creation of an electron without spin flip or hopping [$w^{31}(\hat{\rho}$ and $\hat{\sigma}^z, l=0)$]. Hopping to the nearest-neighbor sites [$w^{31}(\hat{j}$ and $\hat{j}^z, l=1)$] is the next main process. Hopping to the next-nearest-neighbor sites [$w^{31}(\hat{\rho}$ and $\hat{\sigma}^z, l=2)$] is smaller. The mode has contributions mainly from the p-h pair associated with the 16th and 1st local HF orbitals.

The thirteen linear excitations from the 32nd to 44th modes form a branch, $B3$. They have contributions mainly from the p-h pair associated with the 17th local HF orbital and one of the fourteen extended occupied HF orbitals. Each mode on this branch has a main process of hopping to a certain site, which depends on the mode, with or without spin flip. In contrast to the branch $B2$, and contrary to the case of Fig. 1(a), transverse spin modes have odd numbers l and longitudinal spin and charge modes have even numbers l. These are due to the flipped spin density at the location of the hole.

The 45th linear excitation, $L4$, is an antisymmetric *twist* shape mode, as shown in Fig. 4(d), a spatially *localized* transverse spin mode with odd parity. This mode has an energy 4.27. Its main process is hopping to the nearest-neighbor sites with spin flip [$w^{45}(\hat{j}^x$ and $\hat{j}^y, l=1)$], which is due to the flipped spin density at the location of the hole. This mode has contributions mainly from the p-h pairs associated with the 17th and 19th local HF orbitals for particle states and with the 13th and 9th extended HF orbitals for hole states. This mode is also considered to be related to the missing local HF orbital.

The thirteen linear excitations from the 46th to 58th form a branch, $B4$, of almost extended modes. They have contributions mainly from the p-h pair associated with the 18th local HF orbital and one of the fourteen extended occupied HF orbitals. Their processes are similar to those in the modes in the continuum mentioned later. If spins are flipped, they hop to the same sublattice. If not, they hop to the other sublattice. Each mode has weight distributed over all hopping distances l within the even or odd sublattices, but the weight has a maximum on a certain l depending on the mode.

The thirteen linear excitations from the 59th to 71st modes form another branch, $B5$, of almost extended modes. They have contributions mainly from the p-h pair associated with the 19th local HF orbital and one of the fourteen extended occupied HF orbitals. Their processes are similar to those in the modes in the continuum mentioned later. If spins are flipped, they hop to the same sublattice. If not, they hop to the other sublattice. But each mode again has a little preference for the hopping distances l.

The 72nd and 73rd linear excitations, $L5$ and $L6$, are antisymmetric and symmetric *twist* shape modes, respectively, that is, spatially *localized* transverse spin modes with odd and even parities, respectively. They have energies 7.12 and 7.22. Their main process is hopping to the next-nearest-neighbor sites with spin flip [$w^{72}(\hat{j}^x$ and $\hat{j}^y, l=2)$ and $w^{73}(\hat{\sigma}^x$ and $\hat{\sigma}^y, l=2)$]. These modes have contributions mainly from the p-h pairs associated with the 18th and 1st local HF orbitals, and the 19th and 1st local HF orbitals, respectively.

The 164 linear excitations from the 74th to 237th modes, form the continuum, C. The p-h pairs, which contribute to them, are associated with the extended HF orbitals for both particle and hole states. Their processes are similar to the modes in the continuum in the case of Fig. 1(a). If spins are flipped, they hop to the same sublattice. If not, they hop to the other sublattice. Each mode has weight distributed almost uniformly over all hopping distances l within the even or odd sublattices.

The five linear excitations, $B6$, from the 238th to 242nd modes are the *ultragap* modes, their energies ($8.45 \leq \omega_n \leq 8.78$) being similar to those in the case of Fig. 1(a). But their energies are less than the energy difference between the highest and lowest HF orbitals. All of them are extended charge modes, slightly mixed with longitudinal spin modes. The p-h pairs which contribute to them are associated with the extended HF orbitals for both particle and hole states. Their dominant process is charge transfer to the nearest-neighbor sites.

The thirteen linear excitations from the 243rd to 255th modes form another branch, $B7$. They have contributions mainly from the p-h pair associated with one of the thirteen extended unoccupied HF orbitals and the 1st local HF orbital. Each mode on this branch has a main process of hopping to a certain site, which depends on the mode, with or without spin flip. Like the branch $B3$, transverse spin modes have odd numbers l and longitudinal spin and charge modes have even numbers l. These are due to the flipped spin density at the location of the hole.

The highest (255th) linear excitation is a mixed mode of charge and longitudinal spin, which has energy 9.57, almost the same as the energy difference between the highest and lowest HF orbitals. This is because this mode has contributions mainly from the p-h pair associated with the lowest and highest HF orbitals.

The number of linear excitations in the four branches $B2 \sim B5$ is thirteen in each case. On the other hand, the number of the extended occupied HF orbitals is fourteen. The discrepancy between these two numbers may be due to the missing local HF orbital, as indicated when the local HF orbitals are analyzed in the three-site problem (Table I).

C. Comparison with the t-t'-J model

It is interesting to compare the picture obtained in the present RPA with that in the t-t'-J model,[25] which is derived from the large-U Hubbard model. In the t-t'-J model, the process of $O(t\delta)$, where δ is the hole density, is hopping to the nearest-neighbor sites without spin flip only when they are unoccupied. The process of $O(t^2/U)$ is the antiferromagnetic exchange coupling, which appears in the spin-$\frac{1}{2}$ Heisenberg model. The process of $O(t^2\delta/U)$ is hopping to the next-nearest-neighbor sites, with or without spin flip, only when they are unoccupied.

In our case, the hopping to the nearest-neighbor sites without spin flip in the translational shape mode ($n=16$) and the amplitude shape mode ($n=31$) would correspond to the process of $O(t\delta)$ in the t-t'-J model. The hopping to the next-nearest-neighbor sites, with or without spin flip, in the twist modes ($n=72,73$) or translational and amplitude shape modes ($n=16,31$), respectively, would correspond to the process of $O(t^2\delta/U)$ in the t-t'-J model. However, the hopping to the nearest-neighbor sites with spin flip in the antisymmetric twist mode ($n=45$) does not correspond to any bare process in the t-t'-J model.

There are two main differences between the two pictures. First, the RPA studies linear fluctuations around a HF solution. These consist of fluctuation in generalized charge, spin, charge current, and spin current densities. When an electron with a certain spin is hopped from a given site, there is no longer an electron with the same spin left. But, the RPA treats this process only as a change in the densities. Therefore, if the motion of electrons were too slow to compensate the inhomogeneous densities, the RPA would not take so much into account the fact that after hopping there is no electron with the same spin. On the other hand, this is taken in the t-t'-J model. When the on-site correlation limits hopping strongly and the motion of electrons is slow, it would be most direct to approach from the t-t'-J model. Thus the dominant process of the translational and amplitude shape modes, one without spin flip or hopping, may be due to a change in the densities, which is not described by the t-t'-J model.

Second, the elements in the RPA are p-h excitations, some of which have extended character in one or both of the particle and hole states. For example, the main process of the modes in the branch $B2$ is hopping to a certain site. But the hopping distance l is not restricted to small values like $l=0,1,2$ because of extended character in the hole states. Thus, the modes in the continuum C have more extended character. Hopping to different sites within a sublattice occur with almost equal probabilities. By contrast, all the elements in the t-t'-J model are spins which are almost localized due to the constraint imposed on hopping.

The local modes $L1\sim L6$ would contribute to coherent motion of the hole with internal oscillation. However, the modes in the branches $B2\sim B5$ are composites of both local and extended HF orbitals, representing transfer from local (extended) to extended (local) orbitals. They would disturb the coherent motion of the hole, i.e., contribute to incoherent motion. Thus they may be related to the marginality of one-dimensional fermion systems, which are described by the Luttinger liquid.[26] Their behavior in higher dimensions will be of particular interest from this viewpoint.

D. Spectral weights in different susceptibility channels

Hereafter we present the frequency dependence of imaginary parts, $\pi^{-1}\mathrm{Im}\chi_o(q,\omega)$ and $\pi^{-1}\mathrm{Im}\chi_o(l,\omega)$, of susceptibilities,

$$\chi_o(q,\omega)=\sum_l e^{iql}\chi_o(l,\omega)\ , \tag{19}$$

$$\chi_o(l,\omega)=\frac{1}{N}\sum_i\int_{-\infty}^{\infty}dt\, e^{i\omega t}i\langle 0|\mathcal{T}\hat{O}_i(t)\hat{O}_{i+l}|0\rangle\ , \tag{20}$$

respectively, for various Hermitian operators $\hat{O}_i$, where $\hat{O}_i$ is $\hat{\rho}_i$ (charge density), $\hat{\sigma}_i^{\gamma}$ (spin density), $\hat{j}_{i+1,i}$ (charge current), or $\hat{j}_{i+1,i}^{\gamma}$ (spin current). These quantities are easily derived from Eq. (11) for the two-body Green function.

The imaginary parts of susceptibilities at $q=\pi$ are plotted for the transverse spin ($\hat{O}_i=\hat{\sigma}_i^x$ or $\hat{\sigma}_i^y$), longitudinal spin ($\hat{O}_i=\hat{\sigma}_i^z$), and charge ($\hat{O}_i=\hat{\rho}_i$) channels in Figs. 5(a)–5(c), respectively, with the same parameters as in Fig. 1. Each figure shows results in the one-hole system (solid line) as well as in the half-filled system (dashed line). The delta peaks have been broadened with Lorentzians of width 0.001 in (a) and 0.05 in (b) and (c).

In the transverse spin channel [Fig. 5(a)], the Goldstone modes at zero frequency show a large tail in the half-filled system and a much smaller tail in the one-hole system. The Goldstone mode in the one-hole system shows a tail also at other momenta, but that at $q=\pi$ is the largest. The one-hole system has intensity in the low-energy region, whereas the half-filled system does not (on this scale) if the contribution from the Goldstone mode is subtracted.

In both the longitudinal spin and charge channels [Figs. 5(b) and (c)], the half-filled system has intensity only in high-energy regions ($\omega>7.5$). However, the one-hole system has a peak at $\omega=2.7$ in the intermediate-energy region, arising from the amplitude shape mode, and weak intensity in the low-energy region ($1<\omega<2$). This intensity is bleached from the high-energy region, in proportion to the hole density.

In the half-filled system, longitudinal spin excitations and charge excitations are distinguished, and have peaks at different frequencies in the imaginary parts of the respective susceptibilities. However, these excitations are mixed to varying degrees in the one-hole system. In particular, the amplitude shape mode has strongly mixed character of charge and longitudinal spin.

The imaginary part of the longitudinal spin susceptibility at $l=0$ is plotted in Fig. 6, with the same parameters as in Fig. 1. This figure shows results in the one-hole system (solid line) as well as in the half-filled system (dashed

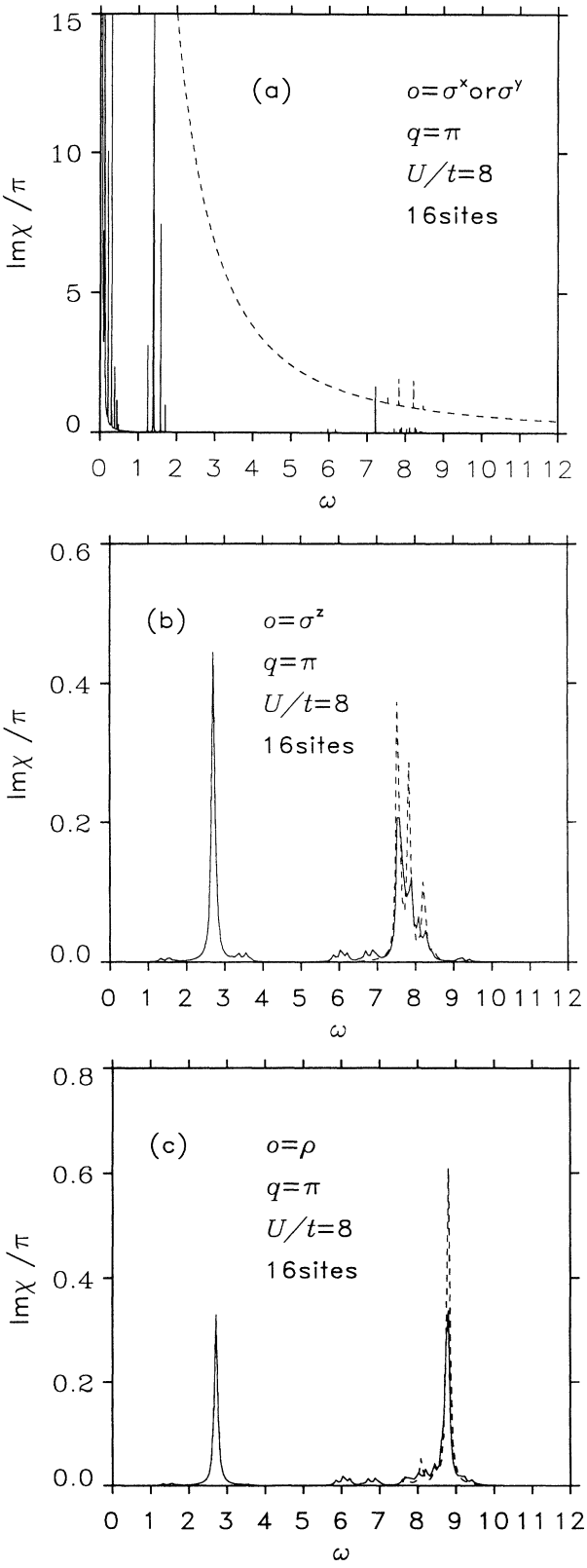

FIG. 5. Spectral weights in $\pi^{-1}\,\mathrm{Im}\chi_o(q=\pi,\omega)$ in the one-hole system (solid line) and in the half-filled system (dashed line) for $U/t=8$ and $N=16$. (a) $\hat{O}_i=\hat{\sigma}_i^x$ or $\hat{\sigma}_i^y$. (b) $\hat{O}_i=\hat{\sigma}_i^z$. (c) $\hat{O}_i=\hat{\rho}_i$.

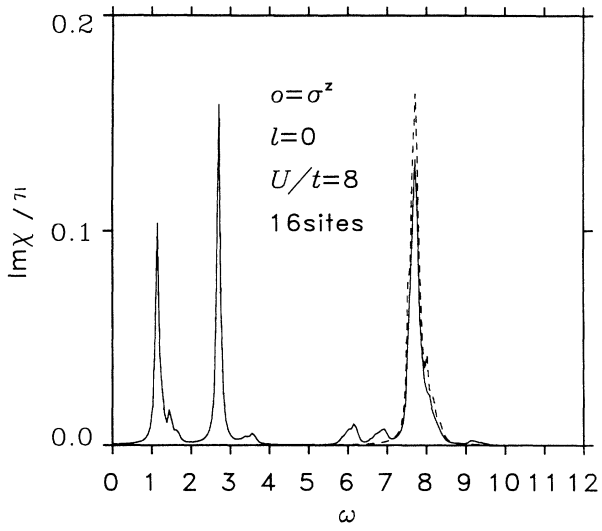

FIG. 6. Spectral weights in $\pi^{-1}\,\mathrm{Im}\chi_o(l=0,\omega)$ in the one-hole system (solid line) and in the half-filled system (dashed line) for $U/t=8$ and $N=16$. $\hat{O}_i=\hat{\sigma}_i^z$.

line), broadened with a Lorentzian of width 0.05. The one-hole system has a peak at $\omega=1.1$, from the translational shape mode and a peak at $\omega=2.7$, from the amplitude shape mode.

The imaginary part of the charge current ($\hat{O}_i=\hat{j}_{i+1,i}$) susceptibility at $q=0$ is plotted in Fig. 7(a), with the same parameters as in Fig. 1. This shows results in the one-hole system (solid line) as well as in the half-filled system (dashed line), broadened with a Lorentzian of width 0.05. The one-hole system has a peak at $\omega=1.1$, from the translational shape mode. This mode would be important for coherent motion of the quasiparticle.

The imaginary part of the transverse spin current ($\hat{O}_i=\hat{j}^x_{i+1,i}$ or $\hat{j}^y_{i+1,i}$) susceptibility at $q=0$ is plotted in Fig. 7(b), with the same parameters as in Fig. 1. This shows results in the one-hole system (solid line) as well as in the half-filled system (dashed line), broadened with a Lorentzian of width 0.05. The one-hole system has a peak at $\omega=4.3$, from the antisymmetric twist shape mode.

The susceptibilities suffer the RPA divergence inherent in the 1D system, as already mentioned. Consequently, their magnitudes may be misleading. However, the overall structure of the frequency dependence of the susceptibilities should give important information on low-lying excitations and their qualitative origins.

The HF solutions violate the discrete translational invariance (defined on the lattice) and the continuous spin rotational invariance, which are known to be preserved in the Bethe-Ansatz solution.[10] However, in the present study of linear excitations around inhomogeneous HF solutions, translational invariance of the system is not restored. It would broaden the positions of the local HF orbitals to form polaron bands, would broaden some of the excitation spectra obtained in the imaginary parts of the susceptibilities, and would make the excitation spec-

trum of charge modes gapless in the thermodynamic limit.

The restoration of the spin rotational invariance would make the lowest spin-wave mode ($q=\pi$) or the Goldstone mode have a finite energy of $O(1/N)$. For the spin-wave theory, introduction of a chemical potential term for the bosons[27] restores the sublattice symmetry, avoids the divergence, and gives good results, close to exact ones, for finite systems even in one dimension.[28] This modified spin-wave theory is closely related to the Schwinger boson technique,[29] as shown in Ref. 28. It is not clear at the present time, however, how this technique can be extended to the finite-U Hubbard model.

V. SUMMARY

In this work all linear excitations have been calculated around HF solutions in the one-dimensional Hubbard model in the RPA. In the half-filled case, the RPA gave good results for the correction to the HF ground-state energy in the large-U regime. The linear excitations consist of the spin-wave modes, the ultragap modes, and the modes in the continuum. The spin-wave modes have spin flip without hopping as a main process, while the ultragap modes have charge transfer to the nearest-neighbor sites. Both of them result from interaction between p-h pairs.

When a hole is introduced into the half-filled system, various HF solutions are obtained including a kink state for small U, a kink-antikink bound state for large U, and a state with a ferromagnetic core around the hole for very large U. Linear excitations are calculated around the kink-antikink bound state in detail. There are five additional branches and six local modes. Each branch has contributions mainly from one of the five local HF orbitals for either particle or hole states. The six local modes consist of a translational shape mode, an amplitude shape mode, two symmetric twist modes, and two antisymmetric twist modes. They have contributions mainly from local HF orbitals for both particle and hole states. The main processes occur locally not only in the spin-wave modes and the ultragap modes but also in the shape modes. Some processes of the shape modes are similar to bare processes in the t-t'-J model. We have also calculated spectral weights in different susceptibility channels and found peaks in the low-energy region, arising from appropriate shape modes.

There are several remaining issues. The zero-frequency modes should be treated differently from finite frequency modes. Tunneling between the states with different locations of the hole should be considered to restore the translational invariance. The two-body Green function should satisfy sum rules, including an f-sum rule,[30] where expectation values are calculated in the exact ground state. Self-energy correction should be calculated for investigation of single-particle properties, after the problem of the divergence (in 1D) in the reduction of the staggered magnetization is solved, which results from the RPA self-energy correction. The validity of the RPA should be tested by exact finite chain methods, especially for $\omega \gtrsim$ the HF excitation gap where our basic approximation is most sensitive to other interactions. We also

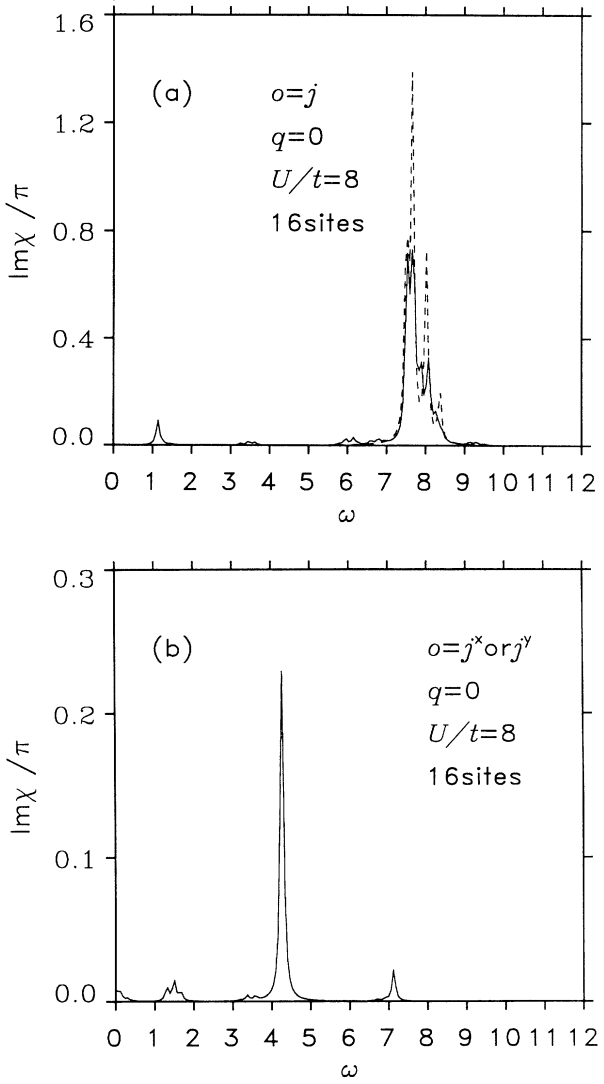

FIG. 7. Spectral weights in $\pi^{-1}\mathrm{Im}\chi_o(q=0,\omega)$ in the one-hole system (solid line) and in the half-filled system (dashed line) for $U/t=8$ and $N=16$. (a) $\hat{O}_i=\hat{j}_{i+1,i}$. (b) $\hat{O}_i=\hat{j}^x_{i+1,i}$ or $\hat{j}^y_{i+1,i}$.

note that a self-trapped exciton will be described well in the present HF plus RPA, but not in the usual homogeneous RPA.

In future work, nearest-neighbor repulsion and electron-phonon interaction will be included—to date effects have been studied mainly for homogeneous HF solutions.[4] The present approach will be applied to multiband extended 1D Hubbard models, which mimic halogen-bridged transition metal linear chain complexes and are considered as one-dimensional analogs of models related to high-temperature superconductors.[31] Above all, application to the two-dimensional Hubbard models is attractive and under study.

ACKNOWLEDGMENTS

We are grateful to Professor Lu Yu for stimulating discussions. This work was supported by the U.S. DOE.

[1]*Proceedings of the Los Alamos Symposium on High Temperature Superconductivity,* Los Alamos, New Mexico, edited by K. S. Bedell, D. Coffey, D. E. Meltzer, D. Pines, and J. R. Schrieffer (Addison-Wesley, Reading, MA, 1990).
[2]B. Johansson and K.-F. Berggren, Phys. Rev. **181**, 855 (1969).
[3]K. Nasu and Y. Toyozawa, J. Phys. Soc. Jpn. **51**, 3111 (1982).
[4]K. Nasu, J. Phys. Soc. Jpn. **53**, 302 (1984).
[5]J. R. Schrieffer, X. G. Wen, and S. C. Zhang, Phys. Rev. Lett. **60**, 944 (1988); Phys. Rev. B **39**, 11 663 (1989).
[6]Z. B. Su, Y. M. Li, W. Y. Lai, and L. Yu, Phys. Rev. Lett. **63**, 1318 (1989).
[7]R. F. Dashen, B. Hasslacher, and A. Neveu, Phys. Rev. D **11**, 3424 (1975).
[8]H. Bergknoff and H. B. Thacker, Phys. Rev. D **19**, 3666 (1979).
[9]M. M. Steiner, R. C. Albers, D. J. Scalapino, and L. J. Sham, Phys. Rev. B **43**, 1637 (1991).
[10]E. H. Lieb and F. Y. Wu, Phys. Rev. Lett. **20**, 1445 (1968).
[11]D. Bohm and D. Pines, Phys. Rev. **92**, 609 (1953).
[12]D. J. Thouless, Nucl. Phys. **22**, 78 (1961).
[13]A. Singh and Z. Tešanović, Phys. Rev. B **41**, 614 (1990).
[14]F. Guinea, E. Louis, and J. A. Vergés (unpublished).
[15]G. E. Brown, *Many-Body Problems* (North-Holland, Amsterdam, 1972).
[16]P. W. Anderson, Phys. Rev. **86**, 694 (1952); R. Kubo, *ibid.* **87**, 568 (1952); T. Oguchi, *ibid.* **117**, 117 (1960).
[17]A. Singh and Z. Tešanović, Phys. Rev. B **41**, 11 457 (1990).
[18]G. Vignale and M. R. Hedayati, Phys. Rev. B **42**, 786 (1990).
[19]S. A. Trugman, Phys. Rev. B **37**, 1597 (1988).
[20]D. M. Frenkel and W. Hanke, Phys. Rev. B **42**, 6711 (1990).
[21]B. I. Shraiman and E. D. Siggia, Phys. Rev. B **40**, 9162 (1989).
[22]Y. Nagaoka, Phys. Rev. **147**, 392 (1966).
[23]J.-P. Blaizot and G. Ripka, *Quantum Theory of Finite Systems* (MIT Press, Massachusetts, 1986).
[24]S. Nakajima, Y. Toyozawa, and R. Abe, *The Physics of Elementary Excitations* (Springer, Berlin, 1980), Chap. 7.
[25]J. E. Hirsch, Phys. Rev. Lett. **54**, 1317 (1985).
[26]J. Sólyom, Adv. Phys. **28**, 201 (1979); V. J. Emery, in *Highly Conducting One-Dimensional Solids,* edited by J. T. Devreese, R. P. Evrard, and V. E. Van Doren (Plenum, New York, 1979).
[27]M. Takahashi, Phys. Rev. Lett. **58**, 168 (1987); J. Phys. Soc. Jpn. **58**, 1524 (1989).
[28]J. E. Hirsch and S. Tang, Phys. Rev. B **39**, 2850 (1989); *ibid.* **40**, 4769 (1989); S. Tang, M. E. Lazzouni, and J. E. Hirsch, *ibid.* **40**, 5000 (1989).
[29]D. P. Arovas and A. Auerbach, Phys. Rev. B **38**, 316 (1988); A. Auerbach and D. P. Arovas, Phys. Rev. Lett. **61**, 617 (1988).
[30]D. Baeriswyl, J. Carmelo, and A. Luther, Phys. Rev. B **33**, 7247 (1986).
[31]J. T. Gammel, I. Batistić, A. R. Bishop, E. Y. Loh, Jr., and S. Marianer, Physica B **163**, 458 (1990).